

Massively scalable stencil algorithm

Mathias Jacquelin[§]
Cerebras Systems Inc.
Sunnyvale, California, USA
mathias.jacquelin@cerebras.net

Mauricio Araya-Polo[§] and Jie Meng
TotalEnergies EP Research & Technology US, LLC.
Houston, Texas, USA
mauricio.araya@totalenergies.com

Abstract—Stencil computations lie at the heart of many scientific and industrial applications. Unfortunately, stencil algorithms perform poorly on machines with cache based memory hierarchy, due to low reuse of memory accesses. This work shows that for stencil computation a novel algorithm that leverages a localized communication strategy effectively exploits the Cerebras WSE-2, which has no cache hierarchy. This study focuses on a 25-point stencil finite-difference method for the 3D wave equation, a kernel frequently used in earth modeling as numerical simulation. In essence, the algorithm trades memory accesses for data communication and takes advantage of the fast communication fabric provided by the architecture. The algorithm—historically memory bound—becomes compute bound. This allows the implementation to achieve near perfect weak scaling, reaching up to 503 TFLOPs on WSE-2, a figure that only full clusters can eventually yield.

Index Terms—Stencil computation, high performance computing, energy, wafer-scale, distributed memory, multi-processor architecture and micro-architecture

I. INTRODUCTION

Stencil computations are central to many scientific problems and industrial applications, from weather forecast ([32]) to earthquake modeling ([19]). The memory access pattern of this kind of algorithm, in which all values in memory are accessed but used in only very few arithmetic operations, is particularly unfriendly to hierarchical memory systems of traditional architectures. Optimizing these memory operations is the main focus of performance improvement research on the topic.

Subsurface characterization is another area where stencils are widely used. The objective is to identify major structures in the subsurface that can either hold hydrocarbon or be used for CO_2 sequestration. One step towards that end is called seismic modeling, where artificial perturbations of the subsurface are modeled solving the wave equation for given initial and boundary conditions. Solving seismic modeling efficiently is crucial for subsurface characterization, since many perturbation sources need to be modeled as the subsurface model iteratively improves. The numerical simulations required by seismic algorithms for field data are extremely demanding, falling naturally in the HPC category and requiring practical evaluation

Traditional architecture	WSE
L1	Memory
L2 & L3	\emptyset
DRAM	\emptyset
Off-node interconnect	Fabric & routers

TABLE I: Equivalences between traditional architectures and the WSE

of technologies and advanced hardware architectures to speed up computations.

Advances in hardware architectures have motivated algorithmic changes and optimizations to stencil applications for at least 20 years ([23]). Unfortunately, the hierarchical memory systems of most current architectures is not well-suited to stencil applications, therefore limiting performance. This applies to multi-core machines, clusters of multi-cores, and accelerator-based platforms such as GPGPUs, FPGAs, etc. ([2], [5]). Alternatively, non-hierarchical architectures were explored in this context, such as the IBM Cell BE ([3]), yielding high computational efficiency but with limited impact.

A key element for large scale simulations is the potential of deploying substantial number of processing units connected by an efficient fabric. The Cell BE lacked the former and it had limited connectivity. Another example of non-hierarchical memory system is the Connection Machine ([12]), which excelled on scaling but at the cost of a very complex connectivity. In this work, a novel stencil algorithm based on localized communications that does not depend on memory hierarchy optimizations is introduced. This algorithm can take advantage of architectures such as the WSE from Cerebras ([4]) and potentially Anton 3-like systems ([28]). These are examples of architectures addressing both limitations described above.

Another angle to be considered is the availability of hardware-based solutions in the market. Literature review yields no generally available hardware architecture addressing the specific bottlenecks of stencil applications. Only a few custom designs examples are available ([10], [14]).

In this work, an implementation of such seismic modeling method on a novel architecture is presented. The proposed mapping requires a complete redesign of the basic stencil algorithm. The contribution of this work is multi-fold:

[§]Equal contribution.

- An efficient distributed implementation of Finite Differences for seismic modeling on a fully-distributed memory architecture with 850,000 processing elements.
- A stencil algorithm that is performance bound to the capacity of individual processing element rather than bound by memory or communication bandwidth.
- The target application ported relies on an industry-validated stencil order.

The paper is organized as follows: Section II reviews relevant contributions in the literature. Section III describes the target application. Section IV provides details of how the target application was redesigned to efficiently use the novel processor architecture. Sections V and VI discuss experimental results and profiling data. Section VII provides discussions and conclusions.

II. RELATED WORK

A. Stencil Computation

Not all stencil computations are the same, and the structure and order of the stencil set the limits of the attainable performance. The higher the order (neighbors to be accounted for) and the closer to a pure star shape is, the harder to compute the stencil is. Traditional hierarchical memory subsystems will be overwhelmed by the memory access pattern which displays very little data reuse. Considerable amount of research effort has been devoted to optimizing stencil computations, and to finding ways around these issues. Spurred by emerging hardware technologies, studies on how stencil algorithms can be tailored to fully exploit unique hardware characteristics have covered many aspects, from DSLs, performance modeling, to pure algorithmic optimizations, targeting low-level architectural features in some cases.

Domain-specific languages (DSLs), domain-specific parallel programming models, and compiler optimizations for stencils have been proposed (e.g., [9], [11], [16], [22]). Performance models have been developed for this computing pattern (see [6], [30]), and the kernel has been ported to a variety of platforms ([2], [3], [5], [35]) including specific techniques to benefit from unique hardware features.

Stencil computations have also been the subject of multiple algorithmic optimizations. Spatial and temporal blocking has been proposed [8], [13], [34]. A further example is the semi-stencil algorithm proposed by De la Cruz et al. [7], which offers an improved memory access pattern and a higher level of data reuse. Promising results are also achieved using a higher dimension cache optimization, as introduced by Nguyen et al. [20], accommodating both thread-level and data-level parallelism. Most recently, Sai et al. [26] studied high-order stencils with a manually crafted collection of implementations of a 25-point seismic modeling stencil in CUDA and HIP for the latest GPGPU hardware. Along this line of hardware-oriented stencil optimizations, Matsumura et al. [17] proposed a frame-

work (*AN5D*) for GPU stencil optimization, obtaining remarkable results.

Wafer-scale computations have first been explored in Rocki et al. [24], in which the authors explore a BiCGStab implementation to solve a linear system arising from a 7-point finite difference stencil on the first generation of Cerebras Wafer-Scale Engine. Albeit computing a much simpler stencil and having a higher arithmetic intensity, this study paved the way to the work presented in this study. A notable difference between the current work and this study is that floating point operations were performed in mixed precision: stencil and AXPY operations being computed using 16 bit floating point operations and global reductions using 32 bit arithmetic. In the present study, only 32 bit floating point arithmetic is used, and neither AXPY operation nor global reductions are involved. This makes the performance achieved by these two applications not directly comparable.

III. FINITE DIFFERENCE FOR SEISMIC MODELING

Minimod is a proxy application that simulates the propagation of waves through the Earth models, by solving a Finite Difference (FD) which is discretized form of the wave equation. It is designed and developed by Total-Energies EP Research & Technologies [18]. *Minimod* is self-contained and designed to be portable across multiple compilers. The application suite provides both non-optimized and optimized versions of computational kernels for targeted platforms. The main purpose is benchmarking of emerging new hardware and programming technologies. Non-optimized versions are provided to allow analysis of pure compiler-based optimizations.

In this work, one of the kernels contained in *Minimod* is used as target for redesign: the acoustic isotropic kernel in a constant-density domain [21]. For this kernel, the wave equation PDE has the following form:

$$\frac{1}{\mathbf{V}^2} \frac{\partial^2 \mathbf{u}}{\partial t^2} - \nabla^2 \mathbf{u} = \mathbf{f}, \quad (1)$$

where $\mathbf{u} = \mathbf{u}(x, y, z)$ is the wavefield, \mathbf{V} is the Earth model (with velocity as the main property), and \mathbf{f} is the source perturbation. The equation is discretized in time using a 2^{nd} order centered stencil, resulting in the semi-discretized equation:

$$\mathbf{u}^{n+1} - \mathbf{Q}\mathbf{u}^n + \mathbf{u}^{n-1} = (\Delta t^2) \mathbf{V}^2 \mathbf{f}^n, \quad (2)$$

with $\mathbf{Q} = 2 + \Delta t^2 \mathbf{V}^2 \nabla^2$.

Finally, the equation is discretized in space using a 25-point stencil in 3D (8^{th} order in space), with four points in each direction as well as the centre point:

$$\begin{aligned} \nabla^2 \mathbf{u}(x, y, z) \approx & \sum_{m=0}^4 c_{xm} [\mathbf{u}(i+m, j, k) + \mathbf{u}(i-m, j, k)] + \\ & c_{ym} [\mathbf{u}(i, j+m, k) + \mathbf{u}(i, j-m, k)] + \\ & c_{zm} [\mathbf{u}(i, j, k+m) + \mathbf{u}(i, j, k-m)] \end{aligned}$$

where c_{xm}, c_{ym}, c_{zm} are discretization parameters, solved in step 4 in Algorithm 1. In the remainder of the document we refer to this operator as the Laplacian.

A simulation in Minimod consists of solving the wave equation at each timestep for thousands of timesteps. Pseudocode of the algorithm is shown in Algorithm 1.

<p>Data: f: source Result: \mathbf{u}^n: wavefield at timestep n, for $n \leftarrow 1$ to T</p> <pre> 1 $\mathbf{u}^0 := 0$; 2 for $n \leftarrow 1$ to T do 3 for each point in wavefield \mathbf{u}^n do 4 Solve Eq. 2 (left hand side) for wavefield \mathbf{u}^n; 5 end 6 $\mathbf{u}^n = \mathbf{u}^n + \mathbf{f}^n$ (Eq. 2 right hand side); 7 end </pre>

Algorithm 1: Minimod high-level description

We note that a full simulation includes additional kernels, such as I/O and boundary conditions. These additional kernels are not evaluated in this study but will be added in the future. The kernel has been ported and optimized for GPGPUs, including NVIDIA A100, full report can be found in [25], this implementation is used as baseline to compare the results with the proposed implementation.

IV. FINITE-DIFFERENCES ON THE WSE

This section introduces general architectural details of the Cerebras Wafer-Scale Engine (WSE) and discusses hardware features allowing the target application to reach the highest level of performance. The mapping of the target algorithm onto the system is then discussed. The implementation is referred to as Finite Differences in the remainder of the study. Communication strategy and core computational parts involved in Finite Differences are also reviewed.

The implementation of Finite Differences on the WSE is written in Cerebras Software Language (*CSL*) using the Cerebras SDK [27], which allows software developers to write custom programs for Cerebras systems. CSL is a C-like language based on Zig [31], a reinterpretation of C which provides a simpler syntax and allows to declare compile-time blocks/optimizations explicitly (rather than relying on macros and the C preprocessor). CSL provides direct access to key hardware features, while allowing the use of higher-level constructs such as functions and while loops. The language allows to express computations and communications across multiple cores. Excerpts provided in the following will use the CSL syntax.

A. The WSE architecture

The WSE is an unprecedented-scale manycore processor. It is the first wafer-scale system [4], embedding all

compute and memory resources within a single silicon wafer, together with a high performance communication interconnect. An overview of the architecture is given in Figure 2. In its latest version, the WSE-2 provides a total of 850,000 processing elements, each with 48 KB of dedicated SRAM memory; up to eight 16-bit floating point operations per cycle; 16 bytes of read and 8 bytes of write bandwidth to the memory per cycle; and a 2D mesh interconnection fabric that can handle 4 bytes of bandwidth per PE per cycle in steady state [15].

The WSE can be seen as an on-wafer distributed-memory machine with a 2D-mesh interconnection *fabric*. This on-wafer network connects *processing elements* or PEs. Each PE has a very fast local memory and is connected to a router. The routers link to the routers of the four neighboring PEs. There is no shared memory. The WSE contains a 7×12 array of identical “dies”, each holding thousands of PEs. Other chips are made by cutting the wafer into individual die. In the WSE, however, the interconnect is extended between dies. This results in a wafer-scale processor tens of times larger than the largest processors on the market at the time of its release.

The instruction set of the WSE is designed to operate on vectors or higher dimensionality objects. This is done by using *data structure descriptors*, which contain information regarding how a particular object should be accessed and operated on (such as address, length, stride, etc.).

As mentioned above, given the distributed memory nature of the WSE, the interconnect plays a crucial role in delivering performance. It is convenient to think of the 2D mesh interconnect in terms of cardinal directions. Each PE has 5 full-duplex links managed by its local router: East, West, North, and South links allow data to reach other routers and PEs, while the *ramp* link allows data to flow between the router and the PE, on which computations can take place. Each link is able to move a 32 bit packet in each direction per cycle. Each unidirectional link operates in an independent fashion, allowing concurrent flow of data in multiple directions.

Every 32 bit packet has a *color* (contained in additional bits of metadata). The role of colors is twofold:

- 1) Colors are used in the routing of communications. A color determines the packet’s progress at each router it encounters from source to destination(s). A router controls, for each color, where — to what subset of the five links — to send a packet of that color. Moreover, colors are akin to virtual channels in which ordering is guaranteed.

- 2) Colors can also be used to indicate the type of a message: a color can be associated to a handler triggered when a packet of that particular color arrives.

The WSE is an unconventional parallel computing machine in the sense that the entire distributed memory machine lies within the same wafer. There is no cache hierarchy nor shared memory. Equivalences between hardware features of the WSE and what they correspond to

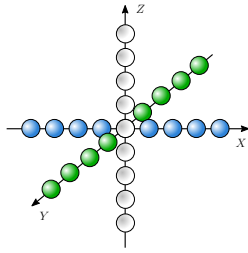


Fig. 1: The 25-point stencil used in Finite Differences. Cells in white (along Z) reside in the local memory of a PE, blue cells are communicated along the X dimension, and green cells are communicated along the Y dimension.

on traditional architectures (such as distributed memory supercomputers) are summarized in Table I.

B. Target Algorithm/application mapping

The sheer scale of the WSE calls for a novel mapping of the target algorithm onto the processor. The 3D $n_x \times n_y \times n_z$ grid on which the stencil computation is performed is mapped onto the WSE in two different ways: the X and Y dimensions are mapped onto the fabric while the Z dimension is mapped into the local memory of a PE. This follows the approach that was explored in Rocki et al. [24], and has the benefit of expressing the highest possible level of concurrency for this particular application. Figure 3a depicts how the domain is distributed over the WSE. Each PE owns a subset of n_z cells of the original grid, as depicted in Figure 3b. In order to simplify the implementation, this local subset is extended by 8 extra cells: 4 cells below and 4 cells above the actual grid. This ensures that any cell in the original grid always has 4 neighbors below and 4 neighbors above. A PE stores the wavefield at two time steps (see Equation 2). In order to lower overheads, computations and communications are performed on blocks of size b . The block size is chosen to be the largest such that the $2 \times (n_z + 8)$ cells and all buffers depending on b can fit in memory.

C. Stencil computation

Computing the spatial component (referred to as the Laplacian) of the governing PDE lies at the heart of the target application, and it is traditionally the most demanding component. In addition to requiring a significant amount of floating point operations, computing the Laplacian also involves data movement, which is known to be very expensive on distributed memory platforms.

In the context of this paper, a 25-point stencil (depicted in Figure 1) is used. The stencil spans over all three dimensions of the grid. In order to compute a particular cell, data from neighboring cells is needed in all three

dimensions. More precisely, a $cell_{x,y,z}$ requires data from neighboring cells:

$$\begin{aligned} cell_{x-4 \leq i < x, y, z}, & \quad cell_{x < i \leq x+4, y, z}, \\ cell_{i, y-4 \leq j < y, z}, & \quad cell_{i, y < j \leq y+4, z}, \\ cell_{i, j, z-4 \leq k < z}, & \quad cell_{i, j, z < k \leq z+4}. \end{aligned}$$

1) *Localized broadcast patterns*: Dimensions X and Y from the grid are mapped onto the fabric of the WSE. To compute the stencil, a PE has therefore to communicate with 4 of its neighbors along each cardinal direction of the PE grid. A communication strategy similar to Rocki et al. [24], in which a single color is used per neighboring PE, would have resulted in an excessive color use for the stencil of interest to this application. In this work, *localized broadcast patterns* along every PE grid directions (*Eastbound* and *Westbound* for the X dimension, and *Northbound* and *Southbound* for the Y dimension) are used instead. Each broadcast pattern uses two dedicated colors (one for receiving data, one for sending data) and can happen concurrently with others broadcast patterns using separate links to communicate between PEs. Given the stencil size used in the application and the number of colors available on the hardware, the limited color usage per broadcast pattern is critical to the feasibility of the implementation.

In each broadcast pattern, multiple *Root* PEs send their local block of data of length b to their respective neighboring 4 processing elements. This pattern is depicted in Figure 4b for the Eastward direction.

The router of each PE is configured to control how packets are received and transmitted. Each router determines, for each color, the incoming links from which that color can be received and the subset of the five outgoing links to which that color will be sent. The routing can be changed at run-time by special commands which can be sent just as other packets are sent. This capability lies at the heart of the communication strategy proposed here. In Figure 4a, the different router configurations used by Finite Differences are given. All *Root* PEs are in configuration 0. Intermediate PEs in each broadcast are in configuration 1, while *Last* PEs are in configuration 2. Ideally, a *Root* PE should broadcast its data only to other PEs. However, due to hardware constraints, a *Root* PE is obliged to receive its own data as well.

After sending its local data, a *Root* PE sends a command to its local router and the following 4 routers. In effect, this routing update shifts the communication pattern by one position: the first neighbor now becomes a *Root* in the next step of the broadcast pattern. After 5 steps (and 5 shifts), a PE has sent its data out and has received data from its 4 neighbors. In Figure 4b, the *target PE* receives data from the West during the first 4 steps, and sends its data to the East at step 5.

One of the very important aspects of this is that changing the routing on a remote router does not require any

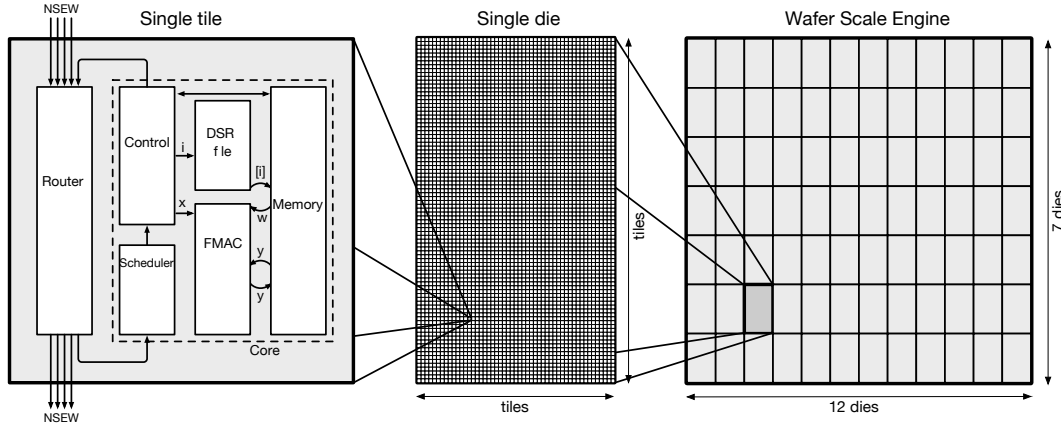


Fig. 2: An overview of the Wafer Scale Engine (WSE). The WSE (to the right) occupies an entire wafer, and is a 2D array of dies. Each die is itself a grid of tiles (in the middle), which contains a router, a processing element and single-cycle access memory (to the left). In total, the WSE-2 embeds 2.6 trillion transistors in a silicon area of 46,225 mm^2 .

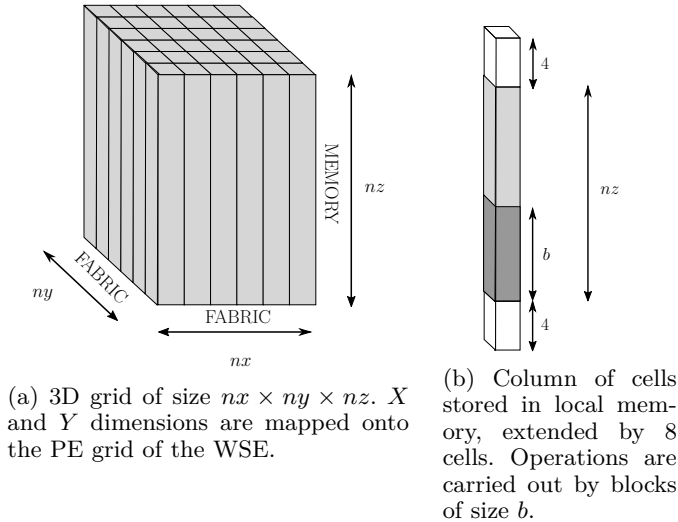


Fig. 3: Computing pattern mapping

action from the local PE. It is therefore uninterrupted and can perform computations simultaneously. Another advantage is that all the control logic is encapsulated in this routing update. A particular PE has to do two things only: sending b cells out, and receiving $5 \times b$ cells (from 4 neighbors and itself). The router configuration will determine when the data flows in or out of a given router. Once a PE is notified that its data has been sent out, it sends a router command to update the routing and transition to the next step of the broadcast pattern. There is no bookkeeping required to determine whether a PE is in a given position in a broadcast.

2) Stencil computation over the X and Y dimensions:

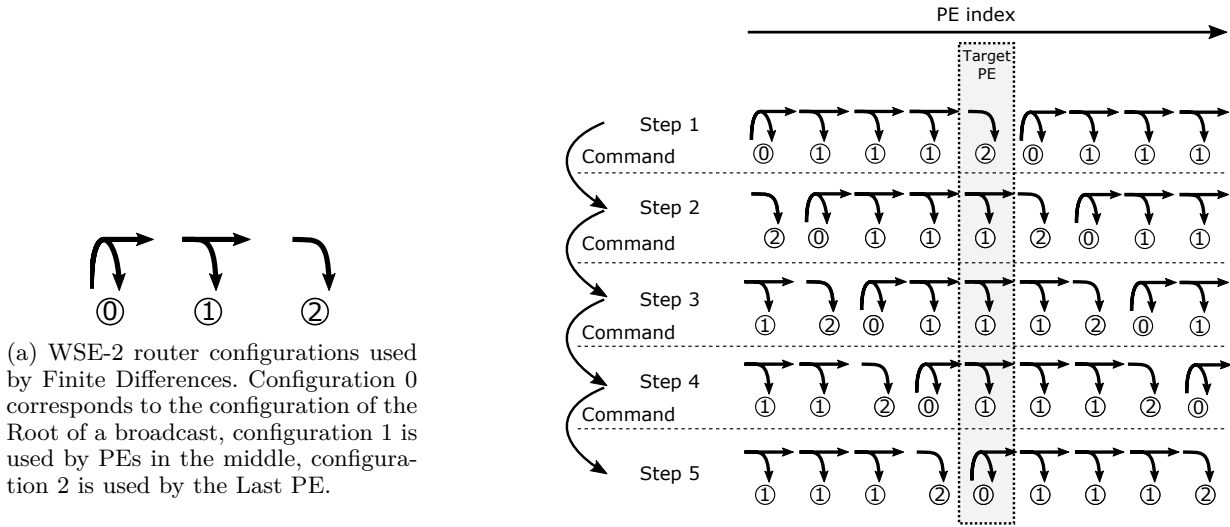
In order to compute the stencil over the X and Y axes, communications between PEs are required. As the stencil involved in this application is a 25-point stencil, data from

16 neighboring PEs along the X and Y directions must be exchanged. This means that at each time step, a PE is involved in 4 localized broadcast patterns (one per cardinal direction). In each broadcast pattern, a PE sends its data and receives data from 4 neighbors.

Using a FMUL instruction, incoming cells from a given direction are multiplied “on the fly” with coefficients depending on their respective distance to the local cell. There are 4 FMUL operations happening concurrently (one per cardinal direction). This is depicted as step 1 in Figure 5 for the data coming from the West. Each FMUL instruction operates on $5 \times b$ incoming cells coming from a particular cardinal direction, and the coefficients (corresponding to c_{xm} and c_{ym} , $\forall m \in \{1 \dots 4\}$ in Section III). A given coefficient is applied to b consecutive cells as they are coming from the same distance neighbor.

Since a PE is receiving data from itself, it is advantageous to compute the contribution from the center $cell_{x,y,z}$ during this step. This is done during the FMUL operation that processes the cells coming from the West, by multiplying the cells coming from the same PE with $c_{x0} + c_{y0} + c_{z0}$. FMULs operating on cells coming from all other directions use a coefficient of 0 for the data coming from the same PE.

Once this distributed computation phase is complete, the data of size $4 \times 5 \times b$ is reduced into a single buffer of b cells (which is referred to as *accumulator*) using a FADD instruction (step 2 in Figure 5). The dimension of size 4 corresponds to the number of localized broadcast patterns a PE participates in, 5 corresponds to the number of PE it is receiving from, and b is the number of elements coming from each PE. All contributions of neighboring cells along the X and Y dimensions are contained in the *accumulator* buffer after the reduction.



(a) WSE-2 router configurations used by Finite Differences. Configuration 0 corresponds to the configuration of the Root of a broadcast, configuration 1 is used by PEs in the middle, configuration 2 is used by the Last PE.

(b) 5 communication steps required to fetch all the data required by a target PE from the West (steps 1 through 4) and to send its data to the East (step 5). Corresponding router configurations are given in the circled numbers. At each step, a router command is sent through the broadcast pattern, changing the configurations of each set of 5 routers.

Fig. 4: Eastward *localized broadcast* operation used in Finite Differences to exchange cells along the X dimension.

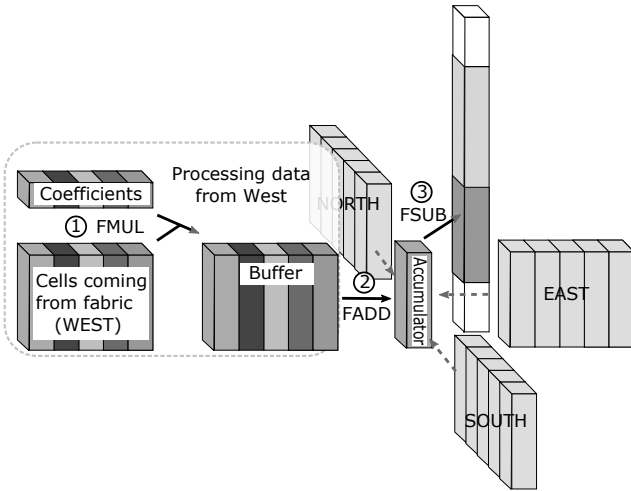


Fig. 5: A summary of main operations: computing the stencil over the X and Y dimensions (for each cardinal direction), reducing the *accumulator* buffer, and subtracting the accumulator from the wavefield.

3) *Stencil computation over the Z dimension*: After remote contributions to the Laplacian from the X and Y axes of the grid have been accumulated, contributions from Z can be computed. Given the problem mapping over the WSE, this means that, at each time step, the computation over the Z dimension can be performed in an embarrassingly parallel fashion since this dimension resides entirely in the memory of a PE.

Each PE executes 8 FMACs instructions of length b , multiplying the wavefield by one of the 8 coefficients

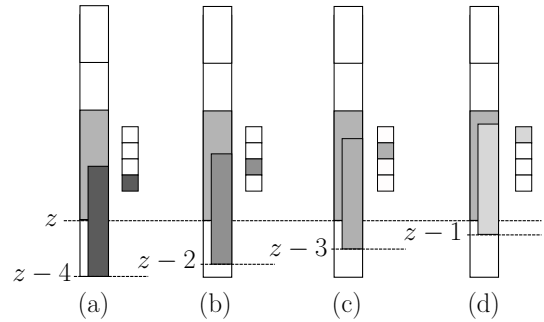


Fig. 6: Applying the stencil over the Z dimension

(corresponding to discretization parameters c_{zm} , $\forall m \in 1 \dots 4$). The result of each FMAC is placed into the *accumulator* buffer (which also contains the contributions from the X and Y dimensions). Given a target block of size b starting at coordinate z_b , each FMAC takes an input block starting at index $z_b + \text{offset}$ and multiplies it by a coefficient. The *offset* values are $\{0, 1, 2, 3\}$ and $\{5, 6, 7, 8\}$, and corresponding coefficients are $\{c_{z4}, c_{z3}, c_{z2}, c_{z1}\}$ and $\{c_{z1}, c_{z2}, c_{z3}, c_{z4}\}$. The CSL code is provided in Figure 7 and the first 4 steps of this process are illustrated in Figure 6. As can be seen, this step skips offset 4, which would correspond to the multiplication by c_{z0} , since that particular computation has already been done as discussed earlier. At the end of this step, the Laplacian is contained in the *accumulator* buffer.

D. Time integration

Once the Laplacian has been computed, the time iteration step given in Equation 2 can happen. The wavefield

$$\begin{aligned}
\text{accumulator}_{z_b \leq i < z_b + b} &= \text{accumulator}_{z_b \leq i < z_b + b} \\
&+ zWF_{z_b - 4 \leq i < z_b + b - 4} \times C_{z4} \\
&+ zWF_{z_b - 3 \leq i < z_b + b - 3} \times C_{z3} \\
&+ zWF_{z_b - 2 \leq i < z_b + b - 2} \times C_{z2} \\
&+ zWF_{z_b - 1 \leq i < z_b + b - 1} \times C_{z1} \\
&+ zWF_{z_b + 1 \leq i < z_b + b + 1} \times C_{z1} \\
&+ zWF_{z_b + 2 \leq i < z_b + b + 2} \times C_{z2} \\
&+ zWF_{z_b + 3 \leq i < z_b + b + 3} \times C_{z3} \\
&+ zWF_{z_b + 4 \leq i < z_b + b + 4} \times C_{z4}
\end{aligned}$$

(a) Operations performed along the Z dimension. zWF is the wavefield stored in the local memory of a PE

```

const accumDsd = @get_dsd(memid_dsd, .{
    .tensor_access = |i|{nz} -> accumulator[i]});
const srcZ0 = @get_dsd(memid_dsd, .{
    .tensor_access = |i|{nz} -> zWF[0, i]});
@fmacs(accumDsd, accumDsd, srcZ0, coefficients[0]);
const srcZ1 = @increment_dsd_offset(srcZ0, 1, f32);
@fmacs(accumDsd, accumDsd, srcZ1, coefficients[1]);
const srcZ2 = @increment_dsd_offset(srcZ0, 2, f32);
@fmacs(accumDsd, accumDsd, srcZ2, coefficients[2]);
const srcZ3 = @increment_dsd_offset(srcZ0, 3, f32);
@fmacs(accumDsd, accumDsd, srcZ3, coefficients[3]);
// srcZ4 not used: update is done in Eastwards broadcast
const srcZ5 = @increment_dsd_offset(srcZ0, 5, f32);
@fmacs(accumDsd, accumDsd, srcZ5, coefficients[5]);
const srcZ6 = @increment_dsd_offset(srcZ0, 6, f32);
@fmacs(accumDsd, accumDsd, srcZ6, coefficients[6]);
const srcZ7 = @increment_dsd_offset(srcZ0, 7, f32);
@fmacs(accumDsd, accumDsd, srcZ7, coefficients[7]);
const srcZ8 = @increment_dsd_offset(srcZ0, 8, f32);
@fmacs(accumDsd, accumDsd, srcZ8, coefficients[8]);

```

(b) Equivalent CSL code. Each `@fmacs` instruction takes an output argument and three input arguments. `@get_dsd` returns a descriptor, corresponding to a *view* of an array. `@increment_dsd_offset` allows to offset the array pointed by an existing descriptor.

Fig. 7: Applying the stencil along the Z dimension.

from the previous time step is added to the *accumulator* buffer. In reality, this is also done during the stencil computation: as mentioned earlier, a PE receives its own data. Doing so allows to use cycles which would have otherwise been wasted.

The next step is to update the wavefield (per Equation 2), by subtracting the wavefield to the *accumulator* buffer (step 3 in Figure 5).

Next, a stimulus, called *source*, needs to be added to a particular cell (with coordinates $(srcX, srcY, srcZ)$) at each time step. The source value at the current time step is added to the wavefield at offset $srcZ$ on the PE with coordinates $(srcX, srcY)$.

V. EXPERIMENTAL EVALUATION

In this section, experimental results of Finite Differences running on a Wafer-Scale Engine are presented. The scalability and energy efficiency achieved by Finite Differences on this massively parallel platform are discussed.

A. Experimental Configuration

The experiments are conducted on two platforms: a Cerebras CS-2 equipped with a WSE-2 chip, and a GPU-based platform used as a reference. The CS-2 is Cerebras' second generation chassis, which uses the 7nm WSE-2 second generation Wafer-Scale Engine. The WSE-2 offers $2.2\times$ more processing elements than the original WSE. The experiments used a fabric of size 755×994 out of the total 850,000 processing elements of the WSE-2. The CS-2 is driven by a Linux server on which no computations take place in the context of this work. The WSE-2 platform uses Cerebras SDK 0.3.0 [27].

The GPU-based platform is *Cypress* from TotalEnergies. It has 4 NVIDIA A100 GPUs, each offering 40 GB of on-device RAM, a 16-core AMD EPYC 7F52 CPU,

and 256 GB of main memory. The GPU platform is using CUDA 11.2 and GCC 8.3.1.

Numerical results produced by Finite Differences on WSE-2 are compared to the results produced by Minimod.

B. Weak scaling Experiments

This section discusses scalability results of Finite Differences on a WSE-2 system. In order to characterize the scalability of Finite Differences, the grid dimension is modified along the X and Y dimensions, while the Z dimension (residing in memory) is kept constant to a relevant value for this type of application. The X and Y dimensions are grown up to a size of 755×994 . Results presented in Table II show the throughput achieved on WSE-2 in Gigacell/s, the wall-clock time required to compute 1,000 time steps on WSE-2, as well as timings on a GPGPU provided as baseline. Timing reported in this section correspond to computations taking place on the device only, be it on GPU or WSE-2.

As can be seen in the table, for all problem sizes, the wall-clock time required on WSE-2 is constant, meaning that Finite Differences scales nearly perfectly on this platform. It is crucial to observe that such a reduction in wall-clock time has a significant impact in practice since this type of computations is repeated hundreds of thousands of times in an industrial context. Finite Differences reaches a throughput of 9872.78 Gcell/s on the largest problem size, which is rarely seen at single system level. This type of throughput is difficult to achieve without using a large number of nodes on distributed-memory supercomputers due to limited strong scalability.

Figure 8 depicts the ratio between the elapsed time achieved by the A100-tuned kernel compared to Finite Differences on WSE-2. As can be seen, when the largest

problem is solved (grid size of $755 \times 994 \times 1000$), a speedup of 228x is achieved. While this number shows great potential, it is understood that using multiple GPUs will likely narrow the gap. However, it is unlikely that such a performance gap can be closed entirely, given the strong scalability issues encountered by this kind of algorithm when using a large number of multi-GPU nodes in HPC clusters ([1], [29]).

Finite Differences shows close to perfect weak scaling on WSE-2. No matter what the grid size is, the run time stays fairly stable. Taking the 200x200 case as a reference, percentages of the ideal weak scaling for various grid sizes are depicted in Figure 9. As can be seen in the plot, Finite Differences systematically reaches over 98% of weak scaling efficiency. This demonstrates how extremely low latency interconnect coupled with local fast memories can be efficiently leveraged by stencil applications relying on a localized communication pattern.

In the next experiment, the sizes of the X and Y dimensions of the grid are fixed to $nx = 755$ and $ny = 994$ while the size of the Z dimension nz is varied from 100 to 1,000. Results presented in Table III show that the throughput increases slightly with nz . This indicates that the implementation gains in efficiency due to larger block sizes b and therefore lower relative overheads. More importantly, it confirms that memory accesses do not limit the performance of the implementation, confirming that it is compute-bound.

nx	ny	nz	Throughput Gcell/s	WSE-2 time [s]	A100 time [s]
200	200	1000	533.64	0.0750	0.7892
400	400	1000	2097.60	0.0763	3.5828
600	600	1000	4731.53	0.0761	8.0000
755	500	1000	4956.17	0.0762	8.5499
755	600	1000	5945.40	0.0762	10.1362
755	900	1000	8922.08	0.0762	15.5070
755	990	1000	9782.14	0.0764	17.4991
755	994	1000	9862.78	0.0761	17.4186

TABLE II: Experimental results for 1,000 time steps for various grid sizes with fixed nz .

nz	b	Throughput Gcell/s	WSE-2 time [s]	Scaling
100	100	8688.76	0.8637	1.0000
200	200	9303.26	1.6133	1.8679
300	300	9492.89	2.3716	2.7458
400	400	9614.15	3.1223	3.6151
500	250	9786.51	3.8342	4.4392
700	350	9885.04	5.3143	6.1531
1000	334	9936.79	7.5524	8.7442

TABLE III: Experimental results, fixed $nx \times ny$ grid dimensions of 755×994 . 100,000 time steps.

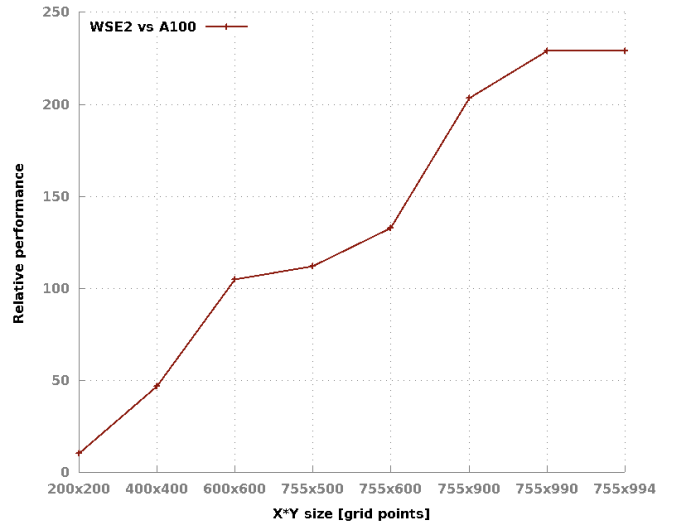


Fig. 8: Comparisons between implementation on WSE-2 and A100 using elapsed time describe in Table II. Fixed $nz = 1000$.

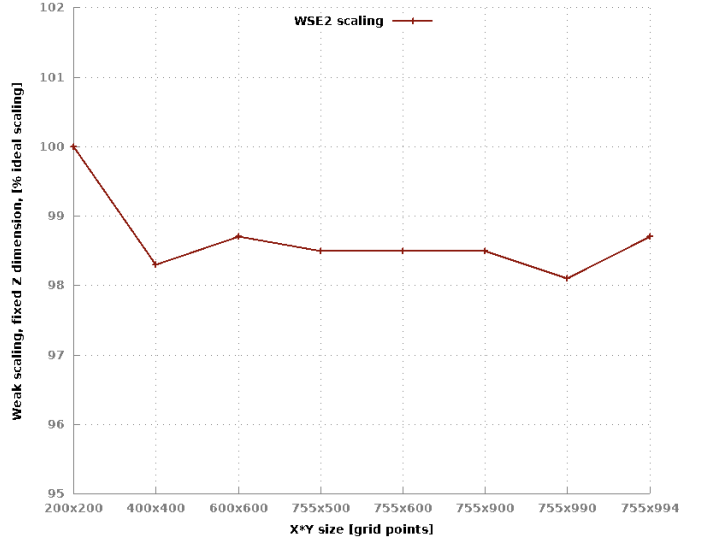


Fig. 9: Weak scaling under assumption that PE memory is fully utilized ($nz = 1000$).

C. Profiling data

In the following, various profiling results are provided for Finite Differences, with the objective to provide general insights on WSE-2-based computations.

Using Cerebras' hardware profiling tool on a $600 \times 600 \times 1000$ grid, the execution of Finite Differences results in an average of 69.6% busy cycles. The 4 PEs at the corners of the grid have 0 busy cycles since they are not doing any computation. There is an average of 11.6% idle cycles caused by memory accesses. As expected, the load is extremely balanced, with a standard deviation of 0.8%. This shows that the hardware is kept busy during the experiment, further confirming the efficiency of the

approach proposed in this work.

The power consumption of the CS-2 during a Finite Differences run on a $755 \times 994 \times 1000$ grid is reported in Figure 10. In order to record a sufficient number of samples, the run time is extended by setting the number of time steps to 10,000,000, leading to a total run time of 754 seconds. The average power consumption during the execution is 22.8 kW, which corresponds to 22 GFLOP/W. Such an energy efficiency is hard to find in the literature for a stencil of this order. In addition to power consumption, Figure 10 also depicts the coolant temperature of the CS-2, which uses a closed-loop water-cooling system. During the execution, the coolant temperature rises very moderately from 23.6°C to a peak of 25.6°C.

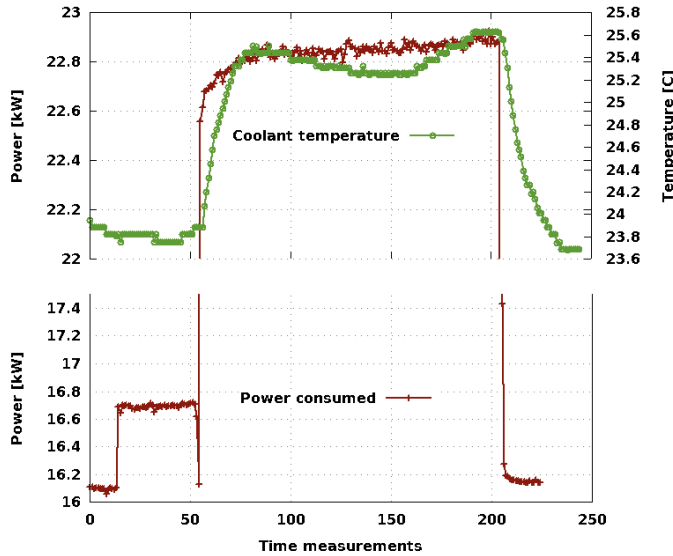


Fig. 10: Power consumption during experiment with grid $755 \times 994 \times 1000$ for 10,000,000 time steps, which amounts to 754 seconds. In the plot, time is subsampled by 3.5 seconds. The power baseline is 16.1 kW and peak is 22.9 kW. Coolant temperature is also reported, with a baseline of 23.6°C and a peak of 25.6°C.

Altogether, experiments show that the Finite Differences algorithm presented in this study is able to exploit low-latency distributed memory architectures such as the WSE-2 with very high hardware utilization. The application has near-perfect weak scalability and provides significant speedups over a reference GPGPU implementation

VI. ROOFLINE MODEL

A roofline model [33] is a synthetic view of how many floating point instructions per cycles can be done. This is the *peak* compute capacity of the platform. However, no computation can be done without loading data: the number of 32 bit words that can be accessed per cycle will also impact the peak compute rate. In the case of a *bandwidth-bound* application, the memory will actually

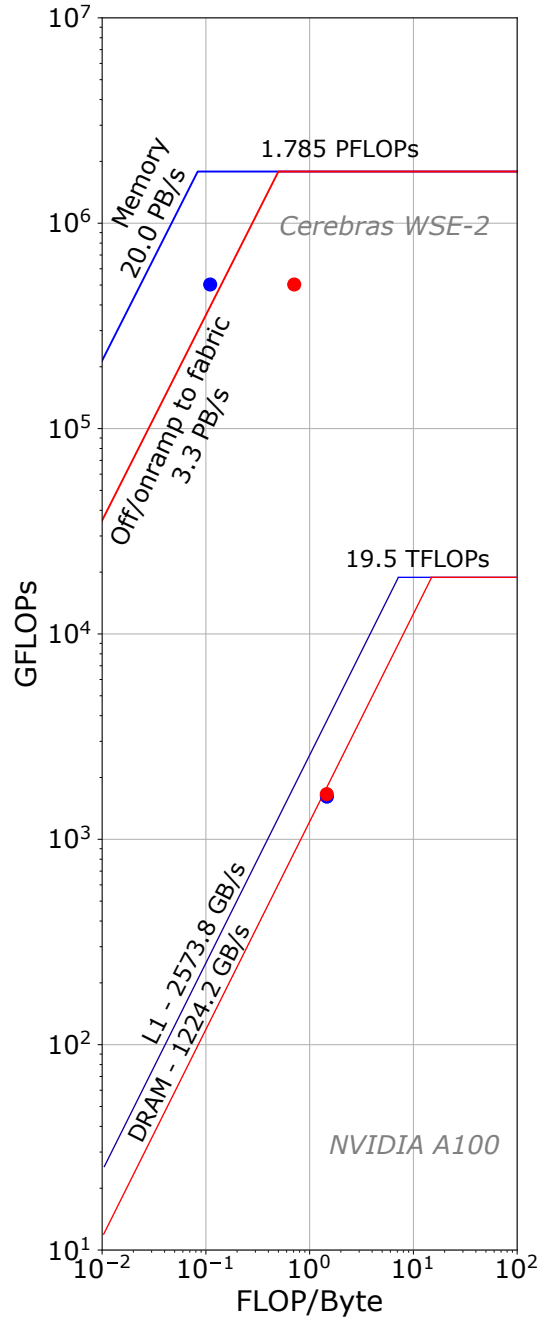


Fig. 11: Roofline models for WSE-2 and GPGPU-based implementations (in log-log scale) for a $755 \times 994 \times 1000$ grid. Dots represent Finite Differences implementations. WSE-2 (top) has two distinct resources: memory and fabric: the leftmost blue dot corresponds to memory accesses, while the red dot to the right corresponds to fabric accesses. Rooflines are given using the same colors. The kernel is clearly in the compute-bound zone for both memory and fabric accesses. On GPGPU (bottom), red dots and lines correspond to DRAM accesses. L1 cache accesses are depicted in blue. The kernel is clearly in the bandwidth-bound zone.

Operation	FLOP	Mem. traffic	Fabric traffic
17 FMUL	1	1/b load, 1 store	1 load
17 FADD	1	2 loads, 1 store	0
8 FMA	2	2 + 1/(b) loads, 1 store	0
1 FSUB	1	2 loads, 1 store	0

TABLE IV: Instruction and memory access counts of the Finite Differences implementation on WSE-2

determine the performance of the overall application. In a similar fashion, accesses to the interconnect can be taken into account when the architecture is a distributed memory platform. This ratio between floating point operations (i.e. the “useful” operations) and the volume of data coming from/going to a given resource, for instance memory, is referred to as *arithmetic intensity* (measured in FLOP/byte).

The WSE-2 is a SIMD-centric multiprocessor providing up to 4 simultaneous 16 bit floating point instructions per cycle. In the context of this work, only 32 bit floating point operations are used. The peak number of floating point operations per second (FLOPs) is represented by the horizontal line at the top of Figure 11.

The WSE-2 does not have a complex cache memory hierarchy: each PE has a single local memory accessed directly. Four 32 bit packets can be accessed from memory per cycle, and up to two packets can be stored to memory per cycle. In memory intensive application, memory limits the peak achievable performance. This corresponds to the slanted blue line at the top of Figure 11.

Each PE is connected to its router by a bi-directional link able to move 32 bits per cycle in each direction (referred to as “off/onramp bandwidth” in the plot). The router is connected to other routers by 4 bi-directional links, each moving 32 bits per cycle. This corresponds to the slanted red line at the top of Figure 11.

For each cell, the stencil computation in Finite Differences involves 25 multiplies and 25 adds. In addition to that, Finite Differences requires a subtraction between the previous time step and the current time step. This corresponds to a total of 51 floating point instructions per cell. As explained in Section IV, due to architecture constraints, only the computation of the stencil along the Z dimension can be done using FMAs. For the X and Y dimensions, the implementation relies on separate FMUL and FADD instructions. The final value of the current time step is computed using a FSUB operation. A summary of the instructions used in Finite Differences, floating point operations per cell, memory traffic, fabric traffic, and instruction count per cell is given in Table IV.

On WSE-2, Finite Differences computes 57 floating point operations per cell, 51 of which are required by the algorithm. Extra operations are due to hardware constraints. The number of operations strictly required by the algorithm is used in all performance numbers. These 51 floating point operations require 112 load and store of 32 bit words from/to memory, and 17 loads from fabric.

This leads to an *arithmetic intensity* of 0.11 with respect to memory accesses, and 0.75 with respect to fabric transfers.

On WSE-2, a $755 \times 994 \times 1000$ grid is computed in 0.0761s (see Table II). This leads to a flop rate of 670.3 MFLOPs per PE, and an aggregated performance of 503 TFLOPs for the entire grid of PEs used by this problem size. The roofline model of the WSE-2, depicted in Figure 11(top), indicates that Finite Differences is *compute bound* thanks to the extremely fast local memory. This is quite remarkable, and confirms the weak scaling results given in Section V. The application is *communication/memory bound* on most architecture, such as the GPU platform used in this study (roofline model depicted in Figure 11(bottom)). Note that different optimizations lead to different arithmetic intensities.

VII. CONCLUSION

In this work, a Finite Differences algorithm taking advantage of low-latency localized communications and flat memory architecture has been introduced. Localized broadcast patterns are introduced to exchange data between processing elements and fully utilize the interconnect. Experiments show that it is possible to reach near perfect weak scalability on distributed memory architecture such as the WSE-2. On this platform, the implementation of Finite Differences reaches 503 TFLOPs. This is a remarkable throughput for this stencil order on a single node machine. The roofline model introduced in this work confirms that Finite Differences becomes compute-bound on the WSE-2. This demonstrates the validity and potential of the approach presented in this work, and demonstrate how different hardware architectures like the WSE-2 can be exploited efficiently by stencil-based applications.

Future efforts include the integration of the ported kernel at the center of more ambitious applications, such as the ones regularly used by seismic modeling experts when taking real-life decisions. Further, given the well established capacity of this hardware architecture for ML-based applications, a hybrid HPC-ML approach will also be investigated.

One interesting consequence of having a relatively compact machine delivering such a high performance level for this type of application is that seismic data processing can happen at the same time it is acquired on the field, which is key when constant monitoring is required. Furthermore, under this scenario, processing capacity can move from data centers closer to where sensors are, namely target edge-HPC.

ACKNOWLEDGEMENTS

Authors would like to thank Cerebras Systems and TotalEnergies for allowing to share the material. Also, authors would like to acknowledge Grace Ho, Ashay Rane, and Natalia Vassilieva from Cerebras for the contributions, and Ruychi Sai from Rice U. for fruitful discussions about GPGPU optimized kernels.

REFERENCES

- [1] O. Anjum, M. Almasri, S. de Gonzalo, and W. Hwu, "An efficient gpu implementation and scaling for higher-order 3d stencils," *Information Sciences*, vol. 586, pp. 326–343, Mar. 2022.
- [2] M. Araya-Polo, J. Cabezas, M. Hanzich, M. Pericas, F. Rubio, I. Gelado, M. Shafiq, E. Morancho, N. Navarro, E. Ayguade, J. M. Cela, and M. Valero, "Assessing accelerator-based hpc reverse time migration," *IEEE Transactions on Parallel and Distributed Systems*, vol. 22, no. 1, pp. 147–162, 2011.
- [3] M. Araya-Polo, F. Rubio, R. de la Cruz, M. Hanzich, J. M. Cela, and D. P. Scarpazza, "3d seismic imaging through reverse-time migration on homogeneous and heterogeneous multi-core processors," *Scientific Programming*, vol. 17, no. 1-2, pp. 185–198, 2009.
- [4] Cerebras, "Wafer-scale deep learning," in *2019 IEEE Hot Chips 31 Symposium (HCS)*. Los Alamitos, CA, USA: IEEE Computer Society, aug 2019, pp. 1–31. [Online]. Available: <https://doi.org/10.1109/HOTCHIPS.2019.8875628>
- [5] K. Datta, S. Kamil, S. Williams, L. Oliker, J. Shalf, and K. Yelick, "Optimization and performance modeling of stencil computations on modern microprocessors," *SIAM Review*, vol. 51, no. 1, pp. 129–159, 2009. [Online]. Available: <https://doi.org/10.1137/070693199>
- [6] R. de la Cruz and M. Araya-Polo, "Towards a multi-level cache performance model for 3d stencil computation," *Procedia Computer Science*, vol. 4, pp. 2146 – 2155, 2011, proceedings of the International Conference on Computational Science, ICCS 2011.
- [7] R. de la Cruz and M. Araya-Polo, "Algorithm 942: Semi-stencil," *ACM Trans. Math. Softw.*, vol. 40, no. 3, 2014.
- [8] M. Frigo and V. Strumpen, "Cache oblivious stencil computations," in *Proceedings of the 19th Annual International Conference on Supercomputing*, ser. ICS '05. New York, NY, USA: Association for Computing Machinery, 2005, p. 361–366.
- [9] S. Ghosh, T. Liao, H. Calandra, and B. M. Chapman, "Experiences with OpenMP, PGI, HMPP and OpenACC directives on ISO/TTI kernels," in *2012 SC Companion: High Performance Computing, Networking Storage and Analysis*, Nov 2012, pp. 691–700.
- [10] F. Gürkaynak and J. Krüger, "Stx – stencil/tensor accelerator factsheet," <https://www.european-processor-initiative.eu/wp-content/uploads/2019/12/EPI-Technology-FS-STX.pdf>, 2019.
- [11] T. Gysi, C. Müller, O. Zinenko, S. Herhut, E. Davis, T. Wicky, O. Fuhrer, T. Hoefler, and T. Grosser, "Domain-specific multi-level ir rewriting for gpu," arXiv:2005.13014, 2020.
- [12] B. Kahle and W. Hillis, *The Connection Machine Model CM-1 Architecture*, ser. Technical report (Thinking Machines Corporation). Thinking Machines Corporation, 1989. [Online]. Available: <https://books.google.com/books?id=PCq7uAAACAAJ>
- [13] S. Kronawitter and C. Lengauer, "Polyhedral search space exploration in the exstencils code generator," *ACM Trans. Archit. Code Optim.*, vol. 15, no. 4, oct 2018. [Online]. Available: <https://doi.org/10.1145/3274653>
- [14] J. Krueger, D. Donofrio, J. Shalf, M. Mohiyuddin, S. Williams, L. Oliker, and F.-J. Pfreund, "Hardware/software co-design for energy-efficient seismic modeling," in *Proceedings of 2011 International Conference for High Performance Computing, Networking, Storage and Analysis*, ser. SC '11. New York, NY, USA: Association for Computing Machinery, 2011. [Online]. Available: <https://doi.org/10.1145/2063384.2063482>
- [15] S. Lie, "Multi-million core, multi-wafer ai cluster," in *2021 IEEE Hot Chips 33 Symposium (HCS)*. IEEE Computer Society, 2021, pp. 1–41.
- [16] M. Louboutin, M. Lange, F. Luporini, N. Kukreja, P. A. Witte, F. J. Herrmann, P. Veleko, and G. J. Gorman, "Devito (v3.1.0): an embedded domain-specific language for finite differences and geophysical exploration," *Geoscientific Model Development*, vol. 12, no. 3, pp. 1165–1187, 2019.
- [17] K. Matsumura, H. R. Zohouri, M. Wahib, T. Endo, and S. Matsuoka, "An5d: Automated stencil framework for high-degree temporal blocking on gpus," in *Proceedings of the 18th ACM/IEEE International Symposium on Code Generation and Optimization*, ser. CGO 2020. New York, NY, USA: Association for Computing Machinery, 2020, p. 199–211.
- [18] J. Meng, A. Atle, H. Calandra, and M. Araya-Polo, "Minimod: A Finite Difference solver for Seismic Modeling," arXiv:2007.06048v1, Jul. 2020. [Online]. Available: <https://arxiv.org/abs/2007.06048v1>
- [19] P. Moczo, J. Kristek, and M. Gális, *The Finite-Difference Modelling of Earthquake Motions: Waves and Ruptures*. Cambridge University Press, 2014.
- [20] A. Nguyen, N. Satish, J. Chhugani, C. Kim, and P. Dubey, "3.5-d blocking optimization for stencil computations on modern cpus and gpus," in *SC '10: Proceedings of the 2010 ACM/IEEE International Conference for High Performance Computing, Networking, Storage and Analysis*, 2010, pp. 1–13.
- [21] A. Qawasmeh, M. R. Hugues, H. Calandra, and B. M. Chapman, "Performance portability in reverse time migration and seismic modelling via openacc," *The International Journal of High Performance Computing Applications*, vol. 31, no. 5, pp. 422–440, 2017.
- [22] P. S. Rawat, M. Vaidya, A. Sukumaran-Rajam, A. Rountev, L. Pouchet, and P. Sadayappan, "On optimizing complex stencils on GPUs," in *2019 IEEE International Parallel and Distributed Processing Symposium (IPDPS)*, 2019, pp. 641–652.
- [23] G. Rivera and C.-W. Tseng, "Tiling optimizations for 3d scientific computations," in *Proceedings of the 2000 ACM/IEEE Conference on Supercomputing*, ser. SC '00. USA: IEEE Computer Society, 2000, p. 32–es.
- [24] K. Rocki, D. Van Essendelft, I. Sharapov, R. Schreiber, M. Morrison, V. Kibardin, A. Portnoy, J. F. Dietiker, M. Syamlal, and M. James, "Fast stencil-code computation on a wafer-scale processor," in *Proceedings of the International Conference for High Performance Computing, Networking, Storage and Analysis*, 2020, pp. 1–14.
- [25] R. Sai, J. Mellor-Crummey, X. Meng, M. Araya-Polo, and J. Meng, "Accelerating high-order stencils on GPUs," in *2020 IEEE/ACM Performance Modeling, Benchmarking and Simulation of High Performance Computer Systems (PMBS)*. Los Alamitos, CA, USA: IEEE Computer Society, nov 2020, pp. 86–108.
- [26] R. Sai, J. Mellor-Crummey, X. Meng, K. Zhou, M. Araya-Polo, and J. Meng, "Accelerating high-order stencils on gpus," *Concurrency and Computation: Practice and Experience*, vol. e6467, 2021.
- [27] J. Selig, "The cerebras software development kit: A technical overview," <https://f.hubspotusercontent30.net/hubfs/8968533/Cerebras%20SDK%20Technical%20Overview%20White%20Paper.pdf>, 2022.
- [28] D. E. Shaw, P. J. Adams, A. Azaria, J. A. Bank, B. Batson, A. Bell, M. Bergdorf, J. Bhatt, J. A. Butts, T. Correia, R. M. Dirks, R. O. Dror, M. P. Eastwood, B. Edwards, A. Even, P. Feldmann, M. Fenn, C. H. Fenton, A. Forte, J. Gagliardo, G. Gill, M. Gorlatova, B. Greskamp, J. Grossman, J. Gullingsrud, A. Harper, W. Hasenplaugh, M. Heily, B. C. Heshmat, J. Hunt, D. J. Ierardi, L. Iserovich, B. L. Jackson, N. P. Johnson, M. M. Kirk, J. L. Klepeis, J. S. Kuskin, K. M. Mackenzie, R. J. Mader, R. McGowen, A. McLaughlin, M. A. Moraes, M. H. Nasr, L. J. Nociolo, L. O'Donnell, A. Parker, J. L. Peticolas, G. Pocina, C. Predescu, T. Quan, J. K. Salmon, C. Schwink, K. S. Shim, N. Siddique, J. Spengler, T. Szalay, R. Tabladillo, R. Tartler, A. G. Taube, M. Theobald, B. Towles, W. Vick, S. C. Wang, M. Wazlowski, M. J. Weingarten, J. M. Williams, and K. A. Yuh, "Anton 3: Twenty microseconds of molecular dynamics simulation before lunch," in *Proceedings of the International Conference for High Performance Computing, Networking, Storage and Analysis*, ser. SC '21. New York, NY, USA: Association for Computing Machinery, 2021. [Online]. Available: <https://doi.org/10.1145/3458817.3487397>
- [29] T. Shimokawabe, T. Endo, N. Onodera, and T. Aoki, "A stencil framework to realize large-scale computations beyond device memory capacity on gpu supercomputers," in *2017 IEEE International Conference on Cluster Computing (CLUSTER)*, 2017, pp. 525–529.
- [30] H. Stengel, J. Treibig, G. Hager, and G. Wellein, "Quantifying performance bottlenecks of stencil computations using the

- execution-cache-memory model,” in *Proceedings of the 29th ACM on International Conference on Supercomputing*, ser. ICS '15. New York, NY, USA: Association for Computing Machinery, 2015, p. 207–216. [Online]. Available: <https://doi.org/10.1145/2751205.2751240>
- [31] Z. team, “Zig programming language,” <https://ziglang.org/>, 2018, (Accessed on 03/18/2022).
- [32] F. Thaler, S. Moosbrugger, C. Osuna, M. Bianco, H. Vogt, A. Afanasyev, L. Mosimann, O. Fuhrer, T. C. Schulthess, and T. Hoefler, “Porting the cosmo weather model to manycore cpus,” in *Proceedings of the Platform for Advanced Scientific Computing Conference*, ser. PASC '19. New York, NY, USA: Association for Computing Machinery, 2019. [Online]. Available: <https://doi.org/10.1145/3324989.3325723>
- [33] S. Williams, A. Waterman, and D. Patterson, “Roofline: An insightful visual performance model for multicore architectures,” *Commun. ACM*, vol. 52, no. 4, p. 65–76, apr 2009. [Online]. Available: <https://doi.org/10.1145/1498765.1498785>
- [34] D. Wonnacott, “Using time skewing to eliminate idle time due to memory bandwidth and network limitations,” in *Proceedings 14th International Parallel and Distributed Processing Symposium. IPDPS 2000*. IEEE, 2000, pp. 171–180.
- [35] K. Zhang, H. Su, P. Zhang, and Y. Dou, “Data layout transformation for stencil computations using arm neon extension,” in *2020 IEEE 22nd International Conference on High Performance Computing and Communications; IEEE 18th International Conference on Smart City; IEEE 6th International Conference on Data Science and Systems (HPCC/SmartCity/DSS)*, 2020, pp. 180–188.